Published in final edited form as:
*Dev Biol*. 2009 October 15; 334(2): 418–428. doi:10.1016/j.ydbio.2009.07.038.

# Caudal regression in adrenocortical dysplasia (*acd*) mice is caused by telomere dysfunction with subsequent p53-dependent apoptosis

**Christopher N. Vlangos**[1], **Bridget C. O'Connor**[1], **Madeleine J. Morley**, **Andrea S. Krause**, **Gail A. Osawa**, and **Catherine E. Keegan**[*]
Department of Pediatrics, University of Michigan, Ann Arbor, MI 48109, USADepartment of Human Genetics, University of Michigan, Ann Arbor, MI 48109, USA

## Abstract

Adrenocortical dysplasia (*acd*) is a spontaneous autosomal recessive mouse mutation that exhibits a pleiotropic phenotype with perinatal lethality. Mutant *acd* embryos have caudal truncation, vertebral segmentation defects, hydronephrosis, and limb hypoplasia, resembling humans with Caudal Regression syndrome. *Acd* encodes Tpp1, a component of the shelterin complex that maintains telomere integrity, and consequently *acd* mutant mice have telomere dysfunction and genomic instability. While the association between genomic instability and cancer is well documented, the association between genomic instability and birth defects is unexplored. To determine the relationship between telomere dysfunction and embryonic malformations, we investigated mechanisms leading to the caudal dysgenesis phenotype of *acd* mutant embryos. We report that the caudal truncation is caused primarily by apoptosis, not altered cell proliferation. We show that the apoptosis and consequent skeletal malformations in *acd* mutants are dependent upon the p53 pathway by genetic rescue of the limb hypoplasia and vertebral anomalies with *p53* null mice. Furthermore, rescue of the *acd* phenotype by p53 deficiency is a dosage-sensitive process, as *acd/acd*, $p53^{-/-}$ double mutants exhibit preaxial polydactyly. These findings demonstrate that caudal dysgenesis in *acd* embryos is secondary to p53-dependent apoptosis. Importantly, this study reinforces a significant link between genomic instability and birth defects.

### Keywords

Caudal regression; Telomere; Apoptosis; p53; Rescue; Development

## Introduction

Adrenocortical dysplasia ($Acd^{acd}$, hereafter denoted *acd*) is a spontaneous autosomal recessive mouse mutation with defects in adrenocortical development (Beamer et al., 1994). The *acd* mutation was originally described in 1994 and is characterized by a postnatal phenotype consisting of hypoplastic adrenal glands that contain enlarged adrenocortical cells with irregular nuclei, growth retardation, skin hyperpigmentation, infertility due to lack of mature germ cells, and hydronephrosis (Beamer et al., 1994; Keegan et al., 2005). On a mixed genetic background with the CAST/Ei strain, approximately 10% of mutants survive past birth although long term survival is reduced (Keegan et al., 2005). On the DW/J strain,



[*]Corresponding author. 1150 W. Medical Center Dr., 3520C MSRB I, Box 5652, Ann Arbor, Michigan 48109-5652, USA. Fax: +1 734 763 9512., keeganc@med.umich.edu (C.E. Keegan).
[1]These authors contributed equally to this work.

the *acd* mutant phenotype is characterized by perinatal lethality, caudal truncation, vertebral segmentation defects, and limb malformations (Keegan et al., 2005), resembling Caudal Regression syndrome (CRS) in humans.

We previously reported that the *acd* mutant phenotype is due to a splicing mutation in the *Acd* gene, which encodes the telomere protein Tpp1 (Keegan et al., 2005). Tpp1 is a component of the shelterin complex, which functions to protect the telomeres from being recognized and processed by the DNA repair machinery and to regulate telomerase access to telomeres (de Lange, 2005). Telomere dysfunction is one mechanism that can give rise to genomic instability, a classic characteristic of tumor cells, which can exhibit aneuploidy due to structurally abnormal chromosomes or abnormal chromosome numbers (Harrington and Robinson, 2002; Zhivotovsky and Kroemer, 2004). RNAi knockdown of *Acd* expression in wildtype mouse embryonic fibroblast (MEF) cells causes telomere dysfunction, leading to p53-mediated growth arrest and an ATM-dependent DNA damage response (Guo et al., 2007). MEF cells from *acd* mutant embryos are deficient in Tpp1 protein at telomeres and exhibit evidence of telomere dysfunction, including an increased number of end-to-end chromosomal fusions, radial structures, and telomere dysfunction-induced foci (Else et al., 2007; Hockemeyer et al., 2007). However, *acd* mutant MEF cells do not exhibit a significant change in telomere length, suggesting that the observed telomere dysfunction is due to uncapping and deprotection rather than telomere shortening (Hockemeyer et al., 2007). The *acd* allele is hypomorphic based on the presence of approximately 2% of appropriately spliced *Acd* mRNA in homozygous *acd* MEF cells, and the worsening of telomere dysfunction in *acd* MEF cells following further RNAi knockdown of *Acd* expression (Else et al., 2007; Hockemeyer et al., 2007).

The pleiotropic phenotype observed in *acd* mutant mice is unique. Null mutations of the majority of shelterin proteins, with the exception of Pot1b, exhibit early embryonic lethality (Celli and de Lange, 2005; Chiang et al., 2004b; Hockemeyer et al., 2006; Karlseder et al., 2003; Wu et al., 2006). While surviving *acd* mutant mice share some phenotypic characteristics with *Pot1b*-null mice, including growth retardation, hyperpigmentation, and germ cell depletion, *Pot1b*-null mice are not known to exhibit embryonic malformations (He et al., 2009; Hockemeyer et al., 2006; Hockemeyer et al., 2008). Additional mutant mouse models exhibiting telomere dysfunction include mice carrying null mutations in both the RNA component (*Terc*) and catalytic reverse transcriptase (*Tert*) component of telomerase (Blasco et al., 1997; Chiang et al., 2004a). However, telomerase deficient mice are viable and fertile for several generations until their telomeres become critically short due to lack of telomerase activity (Lee et al., 1998; Rudolph et al., 1999). An increase in the number of neural tube defects has been reported in late generation telomerase null embryos, but this phenotype more commonly affects the rostral neural tube rather than the caudal region and is not fully penetrant (Herrera et al., 1999).

Caudal Regression syndrome (CRS) is a heterogeneous condition in humans affecting the caudal portion of the embryo that is thought to be caused by both genetic and environmental factors (Bohring et al., 1999). There is a significant amount of overlap between CRS and other caudal defects. In particular, CRS is thought to be part of a phenotypic spectrum that includes VACTERL association (Kallen et al., 2001). VACTERL is a non-random association of birth defects (*v*ertebral anomalies, *a*nal atresia, *c*ardiovascular anomalies, *t*racheo-*e*sophageal fistula, *r*enal anomalies, and preaxial *l*imb anomalies) originally described in 1973 (Quan and Smith, 1973). Both CRS and VACTERL are usually sporadic and are thought to be genetically heterogeneous. However, a small subset of patients with Fanconi anemia (FA) and Rothmund–Thomson syndrome (RTS) exhibits a VACTERL phenotype (Alter et al., 2007; Van Maldergem et al., 2006). While FA and RTS are well known for their role in producing genomic instability and early onset of cancer, the

mechanisms by which genomic instability can lead to congenital malformations in FA and RTS remain unexplored.

In this report, we have characterized the embryonic phenotype of *acd* mutant mice in order to understand the mechanism leading to the caudal truncation phenotype. We hypothesized that the telomere dysfunction caused by the *acd* mutation would lead to increased apoptosis via p53 activation in *acd* mutant embryos. Further, we hypothesized that characteristics of the *acd* phenotype might be rescued when the *acd* mouse line was crossed to mice with a null allele of *Trp53* (hereafter denoted *p53*). Here, we show that *acd* mutant embryos are present in Mendelian ratios during mid-gestation when the caudal portion of the embryo is forming. The *acd* mutant phenotype is evident by embryonic day (E) 9.5 as growth retardation, while the characteristic caudal defects become progressively more pronounced as development proceeds. This is accompanied by a dramatic increase in cellular apoptosis but no significant changes in proliferation. Although *acd* mutant embryos exhibit caudal dysgenesis characterized by vertebral and limb malformations, the process of somitogenesis does not appear to be disrupted. We also demonstrate that the skeletal anomalies and cellular apoptosis observed in *acd* mutant embryos are rescued by p53 deficiency, although the perinatal lethality of the *acd* mutation is not rescued. The *acd* mutant phenotype provides a unique model system for studying the role of telomere dysfunction in the manifestation of birth defects, and our data reveal important insights into the potential mechanisms by which telomere dysfunction and genomic instability can lead to skeletal malformations.

## Materials and methods

### Mice

We have maintained an *acd* breeding colony at the University of Michigan since 2000 when DW/J heterozygous *acd* animals were obtained from cryopreserved stock (stock# 001595) at the Jackson Laboratories, Bar Harbor, ME, USA (Keegan et al., 2005). In order to study strain specific phenotypes, heterozygous *acd* mice were back-crossed to C57BL6/J mice. The data presented here represent embryos from backcross generations N5–N10. *p53* null mice (Jackson Laboratories, Bar Harbor, ME, USA; C57BL6/J; $Trp53^{tm1Tyj}$ stock #002103) were obtained from a breeding stock maintained by the laboratory of Dr. Gary Hammer at the University of Michigan. Mice were housed in specific pathogen free and environmentally controlled conditions with 14 hour light/10 hour dark cycles. Food and water were provided *ad libitum*. All experiments involving mice have been approved by The University of Michigan University Committee on Use and Care of Animals.

### Timed pregnancies

Matings for timed pregnancies were set up using standard animal husbandry techniques. Noon of the day that a vaginal plug was observed was considered E0.5. Embryos were genotyped using DNA isolated from yolk sac as previously described (Keegan et al., 2005; Truett et al., 2000). Chi-squared analysis was performed on litters from the DW/J strain and the C57BL6/J backcross (N5–N7 generation) to determine whether genotypes were present in expected Mendelian ratios. In all experimental settings *acd/acd*, *acd*/+, and +/+ embryos were examined. No phenotypic differences were observed between *acd*/+ and +/+ embryos, consistent with previously published data showing no difference in the cellular phenotype between +/+ and *acd*/+ MEF cells (Hockemeyer et al., 2007). For all experiments, comparisons between *acd* mutant and wildtype embryos were made on littermates.

### Measurement of embryo size

Embryos were photographed under a Leica MZ10 dissecting microscope, and the crown-to-rump length of the embryo was measured on the printed photograph. For each litter, all *acd*

mutant embryos and at least one wildtype embryo were photographed and measured. The percentage of size was calculated by dividing the crown-to-rump length of each mutant by the crown-to-rump length of the wildtype embryo (or average crown-to-rump length when more than one wildtype embryo was photographed) multiplied by 100. Percentages were only calculated on embryos from within one litter that were photographed at the same magnification. The number of litters photographed per timepoint was 5 (E9.5), 9 (E10.5), and 12 (E11.5). Statistical significance was determined using a two-tailed paired student's *t*-test.

### RNA whole mount in situ hybridization

Embryos were dissected in cold PBS, fixed at 4 °C overnight in 4% paraformaldehyde (PFA), rinsed in PBS, dehydrated through a graded methanol series (25%, 50%, 75%, 100%) and stored at −20 °C in 100% methanol until use. RNA whole mount *in situ* hybridization was performed as previously described (Keegan et al., 2005). Digoxigenin-labeled RNA antisense probes for *Acd, Uncx4.1* (Mansouri et al., 1997), *Fgf8* (Sun et al., 2002), *Brachyury* (Wilson et al., 1993), and *Notch1* (Guillemot and Joyner, 1993) were prepared as previously described (Keegan et al., 2005). The *Acd* cRNA probe for whole mount *in situ* hybridization is 286 bp represented by GenBank accession NM_001012638 bases 790 to 1076. The plasmid clone was created by PCR amplification (forward primer: CAGGCTCCAGTCA-GAAGGCTC; reverse primer: AGCTCTGGTCTCACAGGACTG) and cloned into pGEM3Z using standard molecular biology techniques.

### Immunofluorescence on tissue sections

To detect cell proliferation, pregnant mice were injected intraperitoneally with BrdU at 100 mg/g body weight for 1–2 h before embryo removal. Embryos were fixed for 1–2 h at room temperature in 4% PFA, rinsed in PBS, dehydrated in an ethanol series, embedded in paraffin, and sectioned at 7 μm thickness. For immunofluorescence studies sections were deparaffinized in xylene and rehydrated through an ethanol series. Antigen retrieval was performed by boiling tissue for 10 min in 0.01 M sodium citrate. Sections were blocked in 3% bovine serum albumin in PBS and incubated at 4 °C overnight with primary antibody. Sections were counterstained with propidium iodide (PI) diluted at 1:1000–1:4000 or DAPI diluted at 1:1000 (Kirkegaard and Perry Laboratories, Gaithersburg, MD, USA). For BrdU, a polyclonal rat anti-BrdU antibody (Oxford Biotechnology, Raleigh, NC, USA) was used at a 1:200 dilution, followed by fluorescent detection with a donkey anti-rat Alexa Fluor 488 secondary antibody diluted at 1:200 (Invitrogen, Carlsbad, CA, USA). Rabbit polyclonal antibodies were used for Ki67 at 1:500 dilution (Novocastra Laboratories, Newcastle Upon Tyne, UK) and cleaved caspase-3 at 1:400 dilution (Cell Signaling Technology, Danvers, MA, USA) with a biotinylated goat anti-rabbit secondary antibody (Vector Labs, Burlingame, CA, USA) diluted at 1:200. Fluorescent detection was performed using either Cy2- or Cy3-conjugated Streptavidin diluted 1:600 (Jackson Immunoresearch, West Grove, PA, USA). TUNEL analysis was performed using the ApopTag Red *In Situ* Apoptosis Detection Kit as per the manufacturer instructions (Chemicon International, Billerica, MA, USA) with a 10 minute Proteinase K treatment.

### Quantification of immunofluorescence and cell number

Cells were counted in transverse sections using a Leica DMRB microscope 100× objective. Two 100× fields of vision were counted per section with 2 sections counted in total for each embryo. Three wildtype embryos and three *acd/acd* embryos were counted for each timepoint (E9.5, E10.5, and E11.5). Counterstained nuclei and primary antibody-positive cells (Casp-3 or BrdU) were counted in the same field of vision to generate the fraction of positive cells in that field of vision. The number of DAPI- or PI-positive cells was used to

determine the total cell number (used in Fig. 2D). *p*-values were determined using the two-tailed unpaired student's *t*-test.

### p53×acd intercross and skeletal analysis

Heterozygous null *p53* mice were crossed to *acd* heterozygous mice (C57BL/6 background, N8–N10 generation). Resulting double heterozygous mice (*acd*/+, $p53^{+/-}$) were intercrossed to generate double mutant mice (*acd*/*acd*, $p53^{-/-}$). Genotype distributions at weaning age (P21) and E15.5–E16.5 were analyzed by Chi-squared to determine whether the genotypes were present in expected Mendelian ratios. Embryos were dissected at E15.5–E16.5 in fresh PBS and immediately fixed in 95% ethanol for 4 h. Skeletal staining with Alcian Blue and Alizarin Red was performed as previously described (Kimmel and Trammell, 1981). Stained skeletons were analyzed under a Leica MZ7.5 dissecting microscope. The percentage of abnormal/fused vertebrae per embryo was generated by dividing the average number of abnormal/fused vertebrae per embryo by the total number of vertebrae per embryo. An unpaired student's *t*-test was performed to determine statistical significance.

## Results

### The Acd gene is widely expressed in the embryo with relatively higher levels in the limb buds and tail

Little is known about the expression of *Acd*, other than the detection of transcripts in multiple adult tissues and throughout development by northern analysis and RT-PCR (Keegan et al., 2005). The finding that *Acd* encodes a telomeric protein supports the possibility that the gene is expressed ubiquitously. However, because the *acd* embryonic phenotype manifests in the caudal portion of the embryo we hypothesized that *Acd* expression may not be uniform throughout the embryo. To test this hypothesis, we performed whole mount *in situ* hybridization on wildtype embryos using an *Acd* cRNA probe (Fig. 1). At E9.5, we observed widespread expression of the *Acd* gene uniformly throughout the embryo (Fig. 1A). At E11.5, however, we observed a relatively higher concentration of *Acd* mRNA in the neural tube, limb buds, tail, and developing craniofacial region (Fig. 1B). A similar pattern of expression was observed in *acd* mutant embryos at E11.5, although with slightly reduced staining intensity (Fig. 1C). This result was expected as our group has previously shown the presence of *Acd* mRNA in mutant embryos by RT-PCR and northern blot analysis (Keegan et al., 2005). The expression pattern we observed at E11.5 resembles the expression pattern of *Tert* at E11 (Martin-Rivera et al., 1998).

### acd mutant embryos are growth retarded and exhibit reduced cellularity

The *acd* mutation exhibits perinatal lethality and caudal truncation on the DW/J strain (Keegan et al., 2005). Affected $F_2$ animals from a DW/J×C57BL6/J intercross had a similar embryonic phenotype (Keegan et al., 2005). To date we have backcrossed the *acd* mutation onto the C57BL6/J (B6) strain for 10 generations. Data were collected from DW/J embryos and B6 backcross embryos from generations N5–N7, which yields a hypothetical purification of 97–99% B6 DNA. On both the DW/J and B6 strains, we observed Mendelian ratios of mutant embryos from E9.5 to E11.5, during the period of formation of the caudal region (Table 1). Overall, the embryonic phenotype on the B6 strain was similar to the DW/J embryonic phenotype (Keegan et al., 2005). Compared to wildtype littermates, *acd* mutant embryos were growth retarded, although there was some variability in the size of mutant embryos within a litter (Figs. 2A, B). In addition, the caudal truncation phenotype was less pronounced at these early timepoints. Measurement of the crown-to-rump length demonstrated that *acd* mutants were 71.6% (±3.8%) the size of wildtype littermate embryos at E9.5, 77.4% (±1.8%) at E10.5, and 79.1% (±1.4%) at E11.5 (Fig. 2C). The growth retardation phenotype of *acd* mutant embryos suggests a net reduction in cells. To confirm

this, we counted the number of cells per high power field in *acd* embryos versus wildtype littermates, and we found that *acd* mutant embryos do indeed have fewer cells per high power field at E9.5 through E11.5 (Figs. 2C, D, F). Occasional changes in cellular morphology were noted in *acd* mutant embryo sections, including irregularly shaped nuclei, pyknotic nuclei, and nuclear fragments (data not shown). As expected, occasional anaphase bridges were also observed in *acd* mutant tissue sections (data not shown) (Else et al., 2007).

At E8.5, Mendelian genotype ratios were observed. In addition, at E8.5 most *acd* mutant embryos were indistinguishable from wildtype embryos, and the number of somites was in the normal range. In a few litters we observed mild growth retardation in *acd* mutant embryos at E8.5 (data not shown).

## acd mutant embryos exhibit widespread apoptosis but no significant differences in cell proliferation

*Acd* encodes a telomere protein, and cells from *acd* mice exhibit telomere dysfunction, which is known to lead to cell cycle arrest or apoptosis via activation of p53. To detect changes in the number of apoptotic cells, we performed TUNEL staining and immunofluorescence with an antibody to cleaved caspase-3 (Casp-3), a marker of the apoptosis pathway. At E9.5–E11.5, we observed an increase in cells undergoing apoptosis by TUNEL staining and Casp-3 immunofluorescence in mutant embryos compared to wildtype controls (Figs. 3B, D, G, I). Immunofluorescence for the proliferation markers Ki67 or BrdU did not reveal a difference in the number of proliferating cells (Figs. 3E, J). To quantify these observations, we counted Casp-3 positive and BrdU-positive cells from E9.5 through E11.5. This analysis revealed a significant increase in the fraction of Casp-3 positive cells at all timepoints (0.1 vs. 0.02 at E9.5, 0.29 vs. 0.03 at E10.5, 0.22 vs. 0.02 at E11.5, Fig. 3K). There was no difference in the fraction of BrdU-positive cells at E9.5–E11.5 (Fig. 3L). These studies support the hypothesis that apoptosis is the major mechanism leading to reduction of the caudal region of *acd* mutant embryos. Despite the fact that the mutant phenotype appears to be more pronounced in the caudal region of the embryo at E14–16 (Keegan et al., 2005), increased apoptosis was not limited to the caudal region but was widespread throughout the embryo (data not shown). This supports the observed global growth retardation of *acd* mutant embryos (Fig. 2).

## acd mutant embryos exhibit normal somite segmentation and patterning of the caudal region

The presence of vertebral segmentation anomalies in *acd* mutant embryos at E16 suggested the possibility that the process of somitogenesis is disrupted by the *acd* mutation (Keegan et al., 2005). To test this hypothesis, we performed whole mount *in situ* hybridization with several markers of somitogenesis and tail bud development on *acd* mutant and wildtype littermate embryos at E9.5. To investigate the overall patterning of somites, we examined the expression of *Uncx4.1*, which is expressed in the posterior half of each somite (Leitges et al., 2000; Mansouri et al., 2000). At E9.5 we observed normal patterning of *Uncx4.1* expression in the somites of mutant embryos (Figs. 4A, B). Cyclic activation of the Notch signaling pathway is thought to be the signal for somite formation from the presomitic mesoderm (PSM) (Jouve et al., 2000). *Notch*1 is expressed at the boundary of somite formation, followed caudally by a gradient within the PSM (Aulehla et al., 2003). In *acd* mutant embryos at E9.5, we observed a normal pattern of *Notch*1 expression at the somite boundary and PSM, but reduced intensity of expression (Figs. 4C, D). *Fgf8* is expressed in a caudal-to-rostral gradient within the PSM at E9.5 and is thought to represent the somite boundary determination front (Dubrulle et al., 2001). In *acd* mutant embryos, we observed a normal pattern of *Fgf8* expression that included a gradient within the PSM with reduced expression (Figs. 4E, F). Brachyury (*T*), the prototypical T-box gene is first expressed in

tailbud and notochord and is thought to be a direct target of *Wnt3a* in the tailbud (Yamaguchi et al., 1999). We observed a normal pattern of *T* expression in *acd* mutant embryos compared to wildtype littermates (Figs. 4G, H). Taken together, these data indicate that disrupted somitogenesis is not the cause of the caudal dysgenesis phenotype in *acd* mutant embryos.

### p53 deficiency does not rescue the embryonic lethality of acd mutant embryos

To determine whether p53-dependent apoptosis is responsible for the embryonic phenotypes of *acd* mutant embryos, we crossed heterozygous *acd* mice to p53-deficient mice ($p53^{+/-}$) and analyzed the progeny of double heterozygote (*acd*/+, $p53^{+/-}$) intercrosses. We did not detect surviving *acd* mutant mice at weaning age (P21), regardless of p53 genotype (Table 2). A small deficiency of $p53^{-/-}$ mice was observed (Table 2), as expected based on previously published studies of *p53* null mice (Sah et al., 1995). p53 deficiency thus does not rescue the known embryonic lethality of the *acd* mutation on the C57BL/6J strain. Mendelian genotype ratios were observed at E15.5–E16.5 (Table 3), suggesting that the observed lethality is perinatal.

### p53 deficiency results in rescue of hindlimb and vertebral anomalies

Analysis of E15.5–E16.5 skeletons stained with Alcian Blue and Alizarin Red revealed that the majority of *acd/acd*, $p53^{+/+}$ embryos exhibited hypoplasia of the medial digits in at least one hindlimb, occasionally accompanied by an absent tibia, consistent with our previous results (Keegan et al., 2005) (Fig. 5A, Table 4). The majority of *acd/acd*, $p53^{+/-}$ embryos had normal hindlimbs, although some embryos exhibited digit hypoplasia, missing digits, or bifid digits (Fig. 5B, Table 4). No hindlimb abnormalities were observed in *acd*/+, $p53^{-/-}$ or +/+, $p53^{-/-}$ embryos (Table 4). In double mutant (*acd/acd*, $p53^{-/-}$) embryos we observed preaxial (medial) polydactyly or bifid first digits of at least one hindlimb in all embryos (Fig. 5C, Table 4). The majority of embryos had normal forelimbs; however, we did observe absent or hypoplastic digits in a few embryos (Supplementary Table 1). All other embryos had normal limbs (Fig. 5D, Table 4). This suggests that p53-dependent apoptosis in the limb bud is responsible for the limb hypoplasia observed in *acd* mutant embryos. In the absence of p53, there is excess proliferation giving rise to an extra digit.

Vertebral fusions mostly notable in the lumbar region were previously observed in *acd* mutant embryos (Keegan et al., 2005). To our knowledge, vertebral fusions have not been reported previously in p53-deficient mice. We examined the number and morphology of vertebrae by skeletal staining in embryos from double heterozygote intercrosses (Figs. 5E, F, G, H, Supplementary Table 2). In wildtype embryos minor vertebral anomalies were observed in ≤5% of vertebrae suggesting a low level of normal background variation (Figs. 5H, I, Supplementary Table 2). There were multiple vertebral fusion anomalies noted in *acd/acd*, $p53^{+/+}$ embryos (Figs. 5E, I). There was some improvement in *acd/acd*, $p53^{+/-}$ embryos, although they still displayed a significant number of vertebral anomalies (Figs. 5F, I). However, double mutant embryos lacked vertebral fusions and displayed only minor variations similar to background levels, demonstrating complete rescue of this aspect of the *acd* mutant phenotype (Figs. 5G, I, Supplementary Table 2). We also observed a significant number of abnormal vertebrae in *acd*/+, $p53^{-/-}$ embryos, but only occasional abnormalities in *acd*/+, $p53^{+/-}$ and +/+, $p53^{-/-}$ embryos (similar to wildtype embryos), suggesting that gene dosage of either *Acd* or *p53* is important for this effect (Supplementary Table 2). These data demonstrate that a p53-dependent process is responsible for the vertebral fusions in *acd* mutant mice.

Several additional anomalies were more common in embryos with either *acd* mutant or *p53* null genotypes, including unilateral ocular aplasia, mandibular hypoplasia, and exencephaly

(Supplementary Table 3). Mutant *acd* embryos exhibited growth retardation regardless of *p53* genotype, although retardation was less severe in $p53^{+/-}$ and $p53^{-/-}$ embryos compared to $p53^{+/+}$ embryos (data not shown).

### p53 deficiency results in rescue of cellular apoptosis

To confirm that the apoptosis we observed in younger embryos was due to the activation of p53, we performed immunofluorescence for Casp-3 on tissue sections from *acd* mutant and double mutant embryos from the *acd*×*p53* cross. We observed a significant increase in Casp-3 immunofluorescence in *acd/acd*, $p53^{+/+}$ embryos at E10.5, similar to our previous observations in *acd* mutant embryos (Figs. 6D–F). However, in *acd/acd*, $p53^{-/-}$ embryos, we observed background levels of Casp-3 immunofluorescence (Figs. 6G–I), similar to levels observed in wildtype embryos (Figs. 6A–C). These findings confirm that the cellular apoptosis in *acd* mutant embryos is p53-dependent.

## Discussion

In this report, our characterization of the *acd* mutant embryonic phenotype has allowed us to gain new mechanistic insight into the cause of the caudal truncation phenotype. This work clearly reinforces the link between specific birth defects that parallel human malformation syndromes and genomic instability that results from telomere dysfunction, an area that has not previously been studied carefully. We observed a ubiquitous pattern of *Acd* expression in wildtype embryos at E9.5, consistent with the known function of Tpp1 as an integral component of the shelterin telomere complex. We did not examine earlier timepoints by whole mount *in situ* hybridization, though we previously demonstrated the expression of *Acd* mRNA at E7.5 and in ES cells by RT-PCR (Keegan et al., 2005). At E11.5 expression was increased in the limb buds, tail tip, neural tube, and the craniofacial region relative to other tissues. The regions with higher expression correspond to the regions that are most affected in *acd* mutant embryos, and resemble the expression pattern of the enzymatic component of telomerase (*Tert*) during development (Martin-Rivera et al., 1998). This suggests that there are populations of rapidly proliferating cells in these regions with a higher requirement for telomerase and telomere proteins.

We found that *acd* mutant embryos are present in Mendelian ratios during mid-gestation when the caudal portion of the embryo is forming. The *acd* mutant phenotype is visible by embryonic day 9.5 as growth retardation, while the characteristic *acd* caudal truncation becomes more pronounced at later developmental timepoints. The growth retardation is accompanied by a dramatic increase in cellular apoptosis but no significant changes in proliferation. Our previous observation of 0.3 chromosomal fusions per metaphase in *acd* mutant MEF cells is consistent with the extent of apoptosis observed in tissue sections (Else et al., 2007). The observed apoptosis was widespread throughout the embryo rather than restricted to the caudal region, which is consistent with the global growth retardation that we observed at these timepoints. The most likely explanation for the widespread apoptosis in *acd* mutant embryos is that telomere dysfunction causes genomic instability leading to activation of p53 with subsequent apoptosis. Because development proceeds in a rostral-to-caudal fashion, it is possible that the caudal region of the embryo becomes disproportionately affected due to apoptosis of precursor cells that ultimately form the caudal region.

Several mutant mouse models with caudal truncation have previously been described (Greco et al., 1996; Herrmann et al., 1990; Sakai et al., 2001; Takada et al., 1994). Some of these have mutations in genes encoding components of developmental signaling pathways that regulate somitogenesis, the process by which the axial skeleton is formed by partitioning presomitic mesoderm to form somites. This process is accomplished by oscillating

expression of components of the Notch and Wnt signaling pathways, along with opposing gradients of Fgf and retinoic acid signaling that determines the somite segmentation boundary (Aulehla and Herrmann, 2004; Dubrulle and Pourquie, 2004). Although *acd* mutant embryos exhibit caudal dysgenesis with vertebral and limb malformations, somitogenesis is not disrupted, and the expression of representatives of these major signaling pathways is intact. While we previously reported decreased expression of some markers of tail bud development in *acd* mutant embryos at a later timepoint (E11.5), it was unclear whether this was due to a reduction in the number of cells or alterations in the signaling pathways themselves (Keegan et al., 2005). The data presented here establish that the major signaling pathways regulating somitogenesis and tail bud formation are intact, and argue for loss of cells as the mechanism leading to the observed vertebral and limb anomalies.

Telomere dysfunction is known to lead to apoptosis or cell cycle arrest via activation of p53, leading to the hypothesis that p53 deficiency might rescue phenotypes resulting from telomere dysfunction. In late generation *Terc* null mice, p53 deficiency significantly attenuated cell cycle and reproductive organ defects but not the reduced telomere length, and in mice homozygous for a null allele of the telomere repeat binding factor 1 gene (*Terf1*), p53 deficiency partially attenuated the early embryonic lethality (Chin et al., 1999; Karlseder et al., 2003). In other mouse models with genomic instability, p53 deficiency rescues embryonic lethality caused by disruption of the DNA repair genes *Xrcc4* and *DNA ligase IV* and the p53-interacting proteins Mdm2 and Mdm4 (Frank et al., 2000; Gao et al., 2000; Jones et al., 1995; Montes de Oca Luna et al., 1995; Parant et al., 2001). Deficiency of p53 also rescues neural tube defects observed in *splotch* mutant mice, which have loss of function of the *Pax3* transcription factor (Pani et al., 2002). In our cross between *acd* heterozygous and *p53* null mice, we observed a striking rescue of the skeletal anomalies of *acd* mutant embryos as a result of p53 deficiency. This suggests that the vertebral and limb anomalies in *acd* mutants are secondary to p53-dependent apoptosis, and our observed rescue of cellular apoptosis in E10.5 *acd/acd*, $p53^{-/-}$ mutant embryos confirms this as the most likely mechanism. While apoptosis is known to be integral to normal limb development (Zuzarte-Luis and Hurle, 2005), the role of p53-dependent apoptosis has only been studied in the setting of radiation-induced limb malformations (Boreham et al., 2002; Wang et al., 2000). The surprising finding of polydactyly in *acd/acd*, $p53^{-/-}$ embryos suggests the possibility that p53-dependent apoptosis is important during normal limb bud development. However, the absence of limb abnormalities in most *p53* null embryos carrying an *Acd* wildtype allele (26/27 embryos) indicates that telomere dysfunction is required for the polydactyly phenotype. This suggests an alternative explanation that telomere dysfunction in the developing limbs may actually generate a hyperproliferative response that is only apparent when cells are unable to undergo apoptosis. Although the early embryonic lethality of null alleles of other shelterin components precludes analysis, it would be of interest to determine the effect of p53 deficiency on other mouse models with genomic instability, particularly those with embryonic malformations, to determine whether there is indeed a shared mechanism.

p53 deficiency did not rescue the embryonic lethality of the *acd* mutation. Incomplete rescue by p53 deficiency was also observed in embryos harboring a knockout allele of the DNA repair gene *Xrcc2*, although there was a partial rescue of the embryonic phenotype (Adam et al., 2007), similar to *acd* mutant embryos. The reason for lack of complete rescue of the *acd* phenotype is unclear, but could be due to the role of p53-independent pathways that also regulate apoptosis during development or genetic modifiers of the *acd* mutant phenotype. Potential candidates for p53-independent pathways include the p53 related proteins p63 and p73 (Yang et al., 2002), and other pathways known to be involved in apoptosis and

senescence in response to DNA damage, including $p16^{Ink4a}$, $p19^{Arf}$, and ATM (Ju and Rudolph, 2008).

It is clear that p53 plays a role in regulating apoptosis during development. While mice homozygous for a null allele of *p53* can develop normally and survive to adulthood, some *p53* null embryos develop exencephaly and die *in utero* (Sah et al., 1995). Several studies have examined the effect of ionizing radiation, which produces double-stranded DNA breaks, on malformations in p53-deficient mice (Armstrong et al., 1995; Baatout et al., 2002; Bekaert et al., 2005). Malformations including gastroschisis, polydactyly, cleft palate, and growth retardation are significantly increased when fetuses or male parents are exposed to ionizing radiation (Armstrong et al., 1995; Baatout et al., 2002), and telomere shortening is associated with these malformations (Bekaert et al., 2005). *p53* mutations have not been associated with birth defects in humans, but comprehensive studies have not been published.

While telomere dysfunction has been well studied with respect to cancer phenotypes, the study of congenital malformations due to telomere dysfunction has been lacking. Thus, our use of the *acd* mutant mouse model to study birth defects caused by telomere dysfunction is unique. Null alleles of the other components of the shelterin complex, including *Terf2*, *Terf1*, *Pot1a*, and *Tin2*, exhibit early embryonic lethality, rendering the study of developmental phenotypes difficult (Celli and de Lange, 2005; Chiang et al., 2004b; Hockemeyer et al., 2006; Karlseder et al., 2003; Wu et al., 2006). While *Pot1b* null mice and *acd* mutant mice on a mixed genetic background exhibit some phenotypic similarities (He et al., 2009; Hockemeyer et al., 2008), developmental abnormalities have not been reported in *Pot1b* null mice. The contribution of telomere dysfunction to adult phenotypes has been extensively analyzed using telomerase deficient mice with deletion of the *Terc* or *Tert* genes, but the only developmental phenotype reported is an increased incidence in rostral neural tube defects in late generation mutant embryos (Herrera et al., 1999). Telomere dysfunction in telomerase deficient mice is due to critical telomere shortening, which takes several generations to manifest. In contrast, the telomere dysfunction in *acd* mutant mice, which is thought to be due to telomere uncapping and deprotection, is present in the first generation and severity does not increase in later generations.

The caudal truncation, vertebral segmentation anomalies, and limb hypoplasia in *acd* mutant embryos resemble the human phenotypes of Caudal Regression syndrome and VACTERL association. While the genetic causes of CRS and VACTERL association may be heterogeneous, the mechanisms that lead to the constellation of birth defects in CRS and VACTERL are likely to be similar. Although the link between genomic instability, apoptosis, and cancer is well established, our study of the *acd* mouse model reveals that disruption of processes that protect the genome and regulate the disposal of damaged cells during development could be an important contributor to CRS, VACTERL, and potentially other birth defect syndromes. The fact that a ubiquitous process such as maintenance of telomeres results in a tissue specific phenotype may seem surprising on the surface. There are, however, parallels with the well accepted observation that loss of cell cycle regulation and defective genome maintenance have tissue specific consequences for cancer susceptibility. Further study of the developmental phenotypes in *acd* mutant mice will provide mechanistic insight into birth defects that are caused by genomic instability in humans.

## Supplementary Material

Refer to Web version on PubMed Central for supplementary material.

## Acknowledgments

The authors would like to thank Janna Hutz, Maja Adamska, and Erica Macke for technical assistance and Tobias Else for helpful discussions. We also thank Drs. Sally Camper, Tobias Else, Shannon Davis, and Miriam Meisler for critical reading of this manuscript, and Xin Sun (*Fgf8*) and Olivier Pourquie (*Uncx4.1*, *Notch1*, and *T*) for cDNA probes. We acknowledge the DNA Sequencing Core of the University of Michigan's Biomedical Research Core Facilities. Core support was provided by The University of Michigan Cancer Center (CA46592) and the Michigan Diabetes Research and Training Center (DK020572). This work was supported by NIH grant K08-HD42487, a March of Dimes Basil O'Connor Starter Scholar Research Award grant no. 5-FY05-1223, and a March of Dimes Research grant no. 1-FY08-431 to CEK. CNV was supported by a postdoctoral fellowship from the Center for Genetics in Health and Medicine at the University of Michigan.

## References

Adam J, Deans B, Thacker J. A role for Xrcc2 in the early stages of mouse development. DNA Repair (Amst). 2007; 6:224–234. [PubMed: 17116431]

Alter BP, Rosenberg PS, Brody LC. Clinical and molecular features associated with biallelic mutations in FANCD1/BRCA2. J Med Genet. 2007; 44:1–9. [PubMed: 16825431]

Armstrong JF, Kaufman MH, Harrison DJ, Clarke AR. High-frequency developmental abnormalities in p53-deficient mice. Curr Biol. 1995; 5:931–936. [PubMed: 7583151]

Aulehla A, Herrmann BG. Segmentation in vertebrates: clock and gradient finally joined. Genes Dev. 2004; 18:2060–2067. [PubMed: 15342488]

Aulehla A, Wehrle C, Brand-Saberi B, Kemler R, Gossler A, Kanzler B, Herrmann BG. Wnt3a plays a major role in the segmentation clock controlling somitogenesis. Dev Cell. 2003; 4:395–406. [PubMed: 12636920]

Baatout S, Jacquet P, Michaux A, Buset J, Vankerkom J, Derradji H, Yan J, von Suchodoletz H, de Saint-Georges L, Desaintes C, Mergeay M. Developmental abnormalities induced by X-irradiation in p53 deficient mice. In Vivo. 2002; 16:215–221. [PubMed: 12182118]

Beamer WG, Sweet HO, Bronson RT, Shire JG, Orth DN, Davisson MT. Adrenocortical dysplasia: a mouse model system for adrenocortical insufficiency. J Endocrinol. 1994; 141:33–43. [PubMed: 8014601]

Bekaert S, Derradji H, De Meyer T, Michaux A, Buset J, Neefs M, Mergeay M, Jacquet P, Van Oostveldt P, Baatout S. Telomere shortening is associated with malformation in p53-deficient mice after irradiation during specific stages of development. NA Repair (Amst). 2005; 4:1028–1037.

Blasco MA, Lee HW, Hande MP, Samper E, Lansdorp PM, DePinho RA, Greider CW. Telomere shortening and tumor formation by mouse cells lacking telomerase RNA. Cell. 1997; 91:25–34. [PubMed: 9335332]

Bohring A, Lewin SO, Reynolds JF, Voigtlander T, Rittinger O, Carey JC, Kopernik M, Smith R, Zackai EH, Leonard NJ, Gritter HL, Bamforth JS, Okun N, McLeod DR, Super M, Powell P, Mundlos S, Hennekam RC, van Langen IM, Viskochil DH, Wiedemann HR, Opitz JM. Polytopic anomalies with agenesis of the lower vertebral column. Am J Med Genet. 1999; 87:99–114. [PubMed: 10533024]

Boreham DR, Dolling JA, Misonoh J, Mitchel RE. Radiation-induced teratogenic effects in fetal mice with varying Trp53 function: influence of prior heat stress. Radiat Res. 2002; 158:449–457. [PubMed: 12236812]

Celli GB, de Lange T. DNA processing is not required for ATM-mediated telomere damage response after TRF2 deletion. Nat Cell Biol. 2005; 7:712–718. [PubMed: 15968270]

Chiang YJ, Hemann MT, Hathcock KS, Tessarollo L, Feigenbaum L, Hahn WC, Hodes RJ. Expression of telomerase RNA template, but not telomerase reverse transcriptase, is limiting for telomere length maintenance in vivo. Mol Cell Biol. 2004a; 24:7024–7031. [PubMed: 15282303]

Chiang YJ, Kim SH, Tessarollo L, Campisi J, Hodes RJ. Telomere-associated protein TIN2 is essential for early embryonic development through a telomerase-independent pathway. Mol Cell Biol. 2004b; 24:6631–6634. [PubMed: 15254230]

Chin L, Artandi SE, Shen Q, Tam A, Lee SL, Gottlieb GJ, Greider CW, DePinho RA. p53 deficiency rescues the adverse effects of telomere loss and cooperates with telomere dysfunction to accelerate carcinogenesis. Cell. 1999; 97:527–538. [PubMed: 10338216]

de Lange T. Shelterin: the protein complex that shapes and safeguards human telomeres. Genes Dev. 2005; 19:2100–2110. [PubMed: 16166375]

Dubrulle J, Pourquie O. Coupling segmentation to axis formation. Development. 2004; 131:5783–5793. [PubMed: 15539483]

Dubrulle J, McGrew MJ, Pourquie O. FGF signaling controls somite boundary position and regulates segmentation clock control of spatiotemporal Hox gene activation. Cell. 2001; 106:219–232. [PubMed: 11511349]

Else T, Theisen BK, Wu Y, Hutz JE, Keegan CE, Hammer GD, Ferguson DO. Tpp1/Acd maintains genomic stability through a complex role in telomere protection. Chromosome Res. 2007; 15:1001–1013. [PubMed: 18185984]

Frank KM, Sharpless NE, Gao Y, Sekiguchi JM, Ferguson DO, Zhu C, Manis JP, Horner J, DePinho RA, Alt FW. DNA ligase IV deficiency in mice leads to defective neurogenesis and embryonic lethality via the p53 pathway. Mol Cell. 2000; 5:993–1002. [PubMed: 10911993]

Gao Y, Ferguson DO, Xie W, Manis JP, Sekiguchi J, Frank KM, Chaudhuri J, Horner J, DePinho RA, Alt FW. Interplay of p53 and DNA-repair protein XRCC4 in tumorigenesis, genomic stability and development. Nature. 2000; 404:897–900. [PubMed: 10786799]

Greco TL, Takada S, Newhouse MM, McMahon JA, McMahon AP, Camper SA. Analysis of the vestigial tail mutation demonstrates that Wnt3a gene dosage regulates mouse axial development. Genes Dev. 1996; 10:313–324. [PubMed: 8595882]

Guillemot F, Joyner AL. Dynamic expression of the murine Achaete-Scute homologue Mash-1 in the developing nervous system. Mech Dev. 1993; 42:171–185. [PubMed: 8217843]

Guo X, Deng Y, Lin Y, Cosme-Blanco W, Chan S, He H, Yuan G, Brown EJ, Chang S. Dysfunctional telomeres activate an ATM-ATR-dependent DNA damage response to suppress tumorigenesis. EMBO J. 2007; 26:4709–4719. [PubMed: 17948054]

Harrington L, Robinson MO. Telomere dysfunction: multiple paths to the same end. Oncogene. 2002; 21:592–597. [PubMed: 11850784]

He H, Wang Y, Guo X, Ramchandani S, Ma J, Shen MF, Garcia DA, Deng Y, Multani AS, You MJ, Chang S. Pot1b deletion and telomerase haploinsufficiency in mice initiate an ATR-dependent DNA damage response and elicit phenotypes resembling dyskeratosis congenita. Mol Cell Biol. 2009; 29:229–240. [PubMed: 18936156]

Herrera E, Samper E, Blasco MA. Telomere shortening in mTR−/− embryos is associated with failure to close the neural tube. EMBO J. 1999; 18:1172–1181. [PubMed: 10064584]

Herrmann BG, Labeit S, Poustka A, King TR, Lehrach H. Cloning of the T gene required in mesoderm formation in the mouse. Nature. 1990; 343:617–622. [PubMed: 2154694]

Hockemeyer D, Daniels JP, Takai H, de Lange T. Recent expansion of the telomeric complex in rodents: two distinct POT1 proteins protect mouse telomeres. Cell. 2006; 126:63–77. [PubMed: 16839877]

Hockemeyer D, Palm W, Else T, Daniels JP, Takai KK, Ye JZ, Keegan CE, de Lange T, Hammer GD. Telomere protection by mammalian Pot1 requires interaction with Tpp1. Nat Struct Mol Biol. 2007; 14:754–761. [PubMed: 17632522]

Hockemeyer D, Palm W, Wang RC, Couto SS, de Lange T. Engineered telomere degradation models dyskeratosis congenita. Genes Dev. 2008; 22:1773–1785. [PubMed: 18550783]

Jones SN, Roe AE, Donehower LA, Bradley A. Rescue of embryonic lethality in Mdm2-deficient mice by absence of p53. Nature. 1995; 378:206–208. [PubMed: 7477327]

Jouve C, Palmeirim I, Henrique D, Beckers J, Gossler A, Ish-Horowicz D, Pourquie O. Notch signalling is required for cyclic expression of the hairy-like gene HES1 in the presomitic mesoderm. Development. 2000; 127:1421–1429. [PubMed: 10704388]

Ju Z, Rudolph KL. Telomere dysfunction and stem cell ageing. Biochimie. 2008; 90:24–32. [PubMed: 18029082]

Kallen K, Mastroiacovo P, Castilla EE, Robert E, Kallen B. VATER non-random association of congenital malformations: study based on data from four malformation registers. Am J Med Genet. 2001; 101:26–32. [PubMed: 11343333]

Karlseder J, Kachatrian L, Takai H, Mercer K, Hingorani S, Jacks T, de Lange T. Targeted deletion reveals an essential function for the telomere length regulator Trf1. Mol Cell Biol. 2003; 23:6533–6541. [PubMed: 12944479]

Keegan CE, Hutz JE, Else T, Adamska M, Shah SP, Kent AE, Howes JM, Beamer WG, Hammer GD. Urogenital and caudal dysgenesis in adrenocortical dysplasia (acd) mice is caused by a splicing mutation in a novel telomeric regulator. Hum Mol Genet. 2005; 14:113–123. [PubMed: 15537664]

Kimmel CA, Trammell C. A rapid procedure for routine double staining of cartilage and bone in fetal and adult animals. Stain Technol. 1981; 56:271–273. [PubMed: 6171056]

Lee HW, Blasco MA, Gottlieb GJ, Horner JW 2nd, Greider CW, DePinho RA. Essential role of mouse telomerase in highly proliferative organs. Nature. 1998; 392:569–574. [PubMed: 9560153]

Leitges M, Neidhardt L, Haenig B, Herrmann BG, Kispert A. The paired homeobox gene Uncx4.1 specifies pedicles, transverse processes and proximal ribs of the vertebral column. Development. 2000; 127:2259–2267. [PubMed: 10804169]

Mansouri A, Yokota Y, Wehr R, Copeland NG, Jenkins NA, Gruss P. Paired-related murine homeobox gene expressed in the developing sclerotome, kidney, and nervous system. Dev Dyn. 1997; 210:53–65. [PubMed: 9286595]

Mansouri A, Voss AK, Thomas T, Yokota Y, Gruss P. Uncx4.1 is required for the formation of the pedicles and proximal ribs and acts upstream of Pax9. Development. 2000; 127:2251–2258. [PubMed: 10804168]

Martin-Rivera L, Herrera E, Albar JP, Blasco MA. Expression of mouse telomerase catalytic subunit in embryos and adult tissues. Proc Natl Acad Sci U S A. 1998; 95:10471–10476. [PubMed: 9724727]

Montes de Oca Luna R, Wagner DS, Lozano G. Rescue of early embryonic lethality in mdm2-deficient mice by deletion of p53. Nature. 1995; 378:203–206. [PubMed: 7477326]

Pani L, Horal M, Loeken MR. Rescue of neural tube defects in Pax-3-deficient embryos by p53 loss of function: implications for Pax-3-dependent development and tumorigenesis. Genes Dev. 2002; 16:676–680. [PubMed: 11914272]

Parant J, Chavez-Reyes A, Little NA, Yan W, Reinke V, Jochemsen AG, Lozano G. Rescue of embryonic lethality in Mdm4-null mice by loss of Trp53 suggests a nonoverlapping pathway with MDM2 to regulate p53. Nat Genet. 2001; 29:92–95. [PubMed: 11528400]

Quan L, Smith DW. The VATER association. Vertebral defects, anal atresia, T-E fistula with esophageal atresia, radial and renal dysplasia: a spectrum of associated defects. J Pediatr. 1973; 82:104–107. [PubMed: 4681850]

Rudolph KL, Chang S, Lee HW, Blasco M, Gottlieb GJ, Greider C, DePinho RA. Longevity, stress response, and cancer in aging telomerase-deficient mice. Cell. 1999; 96:701–712. [PubMed: 10089885]

Sah VP, Attardi LD, Mulligan GJ, Williams BO, Bronson RT, Jacks T. A subset of p53-deficient embryos exhibit exencephaly. Nat Genet. 1995; 10:175–180. [PubMed: 7663512]

Sakai Y, Meno C, Fujii H, Nishino J, Shiratori H, Saijoh Y, Rossant J, Hamada H. The retinoic acid-inactivating enzyme CYP26 is essential for establishing an uneven distribution of retinoic acid along the anterio-posterior axis within the mouse embryo. Genes Dev. 2001; 15:213–225. [PubMed: 11157777]

Sun X, Mariani FV, Martin GR. Functions of FGF signalling from the apical ectodermal ridge in limb development. Nature. 2002; 418:501–508. [PubMed: 12152071]

Takada S, Stark KL, Shea MJ, Vassileva G, McMahon JA, McMahon AP. Wnt3a regulates somite and tailbud formation in the mouse embryo. Genes Dev. 1994; 8:174–189. [PubMed: 8299937]

Truett GE, Heeger P, Mynatt RL, Truett AA, Walker JA, Warman ML. Preparation of PCR-quality mouse genomic DNA with hot sodium hydroxide and tris (HotSHOT). Biotechniques. 2000; 29 (52):54. [PubMed: 10907077]

Van Maldergem L, Siitonen HA, Jalkh N, Chouery E, De Roy M, Delague V, Muenke M, Jabs EW, Cai J, Wang LL, Plon SE, Fourneau C, Kestila M, Gillerot Y, Megarbane A, Verloes A. Revisiting the craniosynostosis-radial ray hypoplasia association: Baller–Gerold syndrome caused by mutations in the RECQL4 gene. J Med Genet. 2006; 43:148–152. [PubMed: 15964893]

Wang B, Ohyama H, Haginoya K, Odaka T, Yamada T, Hayata I. Prenatal radiation-induced limb defects mediated by Trp53-dependent apoptosis in mice. Radiat Res. 2000; 154:673–679. [PubMed: 11096424]

Wilson V, Rashbass P, Beddington RS. Chimeric analysis of T (Brachyury) gene function. Development. 1993; 117:1321–1331. [PubMed: 8404534]

Wu L, Multani AS, He H, Cosme-Blanco W, Deng Y, Deng JM, Bachilo O, Pathak S, Tahara H, Bailey SM, Behringer RR, Chang S. Pot1 deficiency initiates DNA damage checkpoint activation and aberrant homologous recombination at telomeres. Cell. 2006; 126:49–62. [PubMed: 16839876]

Yamaguchi TP, Takada S, Yoshikawa Y, Wu N, McMahon AP. T (Brachyury) is a direct target of Wnt3a during paraxial mesoderm specification. Genes Dev. 1999; 13:3185–3190. [PubMed: 10617567]

Yang A, Kaghad M, Caput D, McKeon F. On the shoulders of giants: p63, p73 and the rise of p53. Trends Genet. 2002; 18:90–95. [PubMed: 11818141]

Zhivotovsky B, Kroemer G. Apoptosis and genomic instability. Nat Rev Mol Cell Biol. 2004; 5:752–762. [PubMed: 15340382]

Zuzarte-Luis V, Hurle JM. Programmed cell death in the embryonic vertebrate limb. Semin Cell Dev Biol. 2005; 16:261–269. [PubMed: 15797836]

## Appendix A. Supplementary data

Supplementary data associated with this article can be found, in the online version, at doi: 10.1016/j.ydbio.2009.07.038.

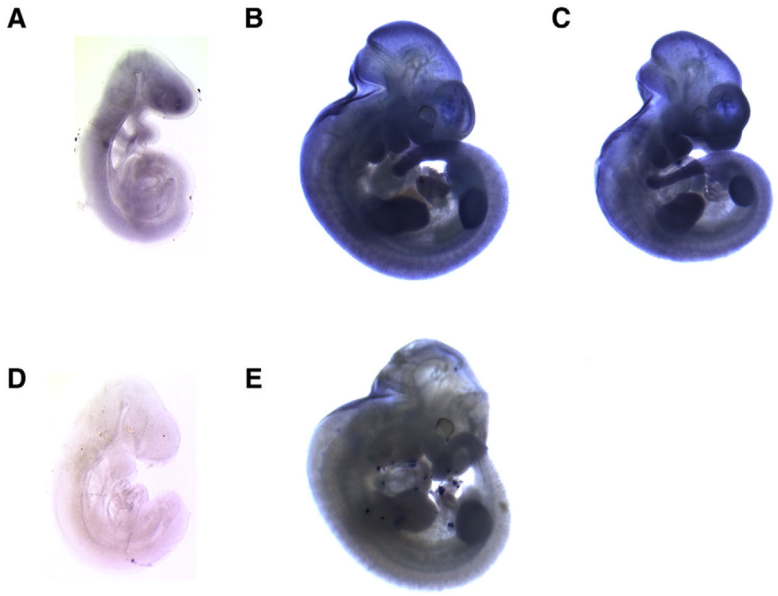


**Fig. 1.**
*Acd* is expressed ubiquitously during embryogenesis. Wildtype (A, B, D, E) and *acd* mutant (C) embryos hybridized with digoxigenin labeled *Acd* antisense RNA probe (A–C) or *Acd* sense control probe (D, E).

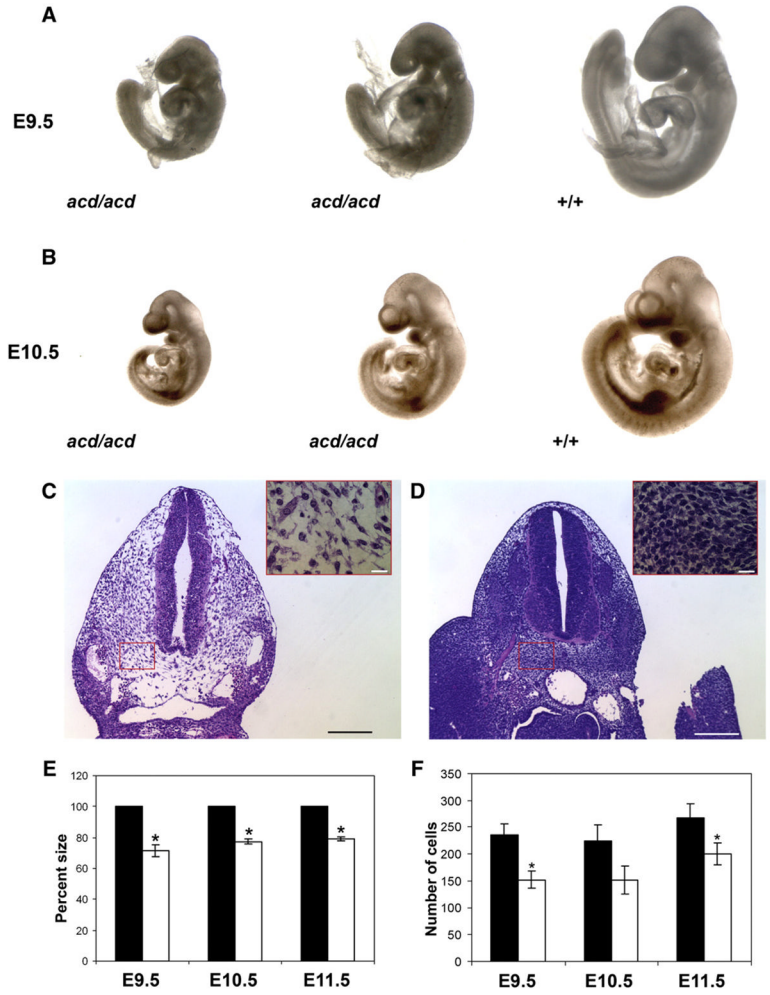


**Fig. 2.**

*acd* mutant embryos are growth retarded and exhibit reduced cellularity. Comparison of *acd* mutant and wildtype littermates at (A) E9.5 and (B) E10.5 shows growth retardation of mutant embryos. H & E photograph of *acd* mutant (C) and wildtype (D) tissue sections shows reduced cellularity in *acd* mutant mesenchyme. Insets depict high power magnification of the boxed area representing a typical area in which cell numbers were counted. Scale bars represent 100 μm in low power figure and 20 μm in high power inset. (E) Calculation of percent size of wildtype littermates demonstrates statistically significant reduction in size of *acd* mutant embryos at all timepoints. *Represents $p<0.001$ by student's *t*-test. (F) Quantification of number of cells per high power field reveals a statistically significant decrease in cell number in *acd* mutant embryos at E9.5 and E11.5. *Represents $p<0.05$ by student's *t*-test.

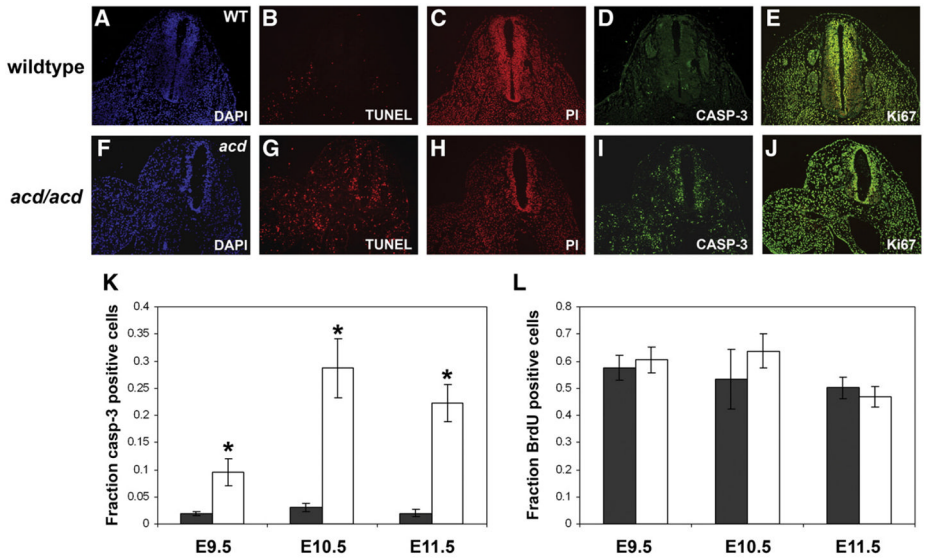


**Fig. 3.**

*acd* mutant embryos exhibit increased apoptosis. Transverse sections of wildtype (A–E) and mutant (F–J) *acd* embryos at E11.5. TUNEL staining (B, G) and cleaved caspase-3 immunohistochemistry (D, I) show an increase in the number of apoptotic cells in *acd* mutant embryos (G, I). A and F show DAPI counterstain of section in panel B and G, respectively, and C and H show propidium iodide (PI) counterstain of section in panel D and I, respectively. (E, J) Immunohistochemistry for Ki67 (green) with propidium iodide (red) counterstain shows no significant difference in the number of proliferating cells in WT (E) vs. *acd* mutant (J) embryos. (K) Average fraction of caspase-3 positive cells in wildtype (black) and *acd* mutant (white) embryos is significantly different at all timepoints. *Denotes $p<0.001$ by student's *t*-test. (L) Average fraction of BrdU-positive cells in wildtype (black) and *acd* mutant (white) embryos shows no statistically significant differences.

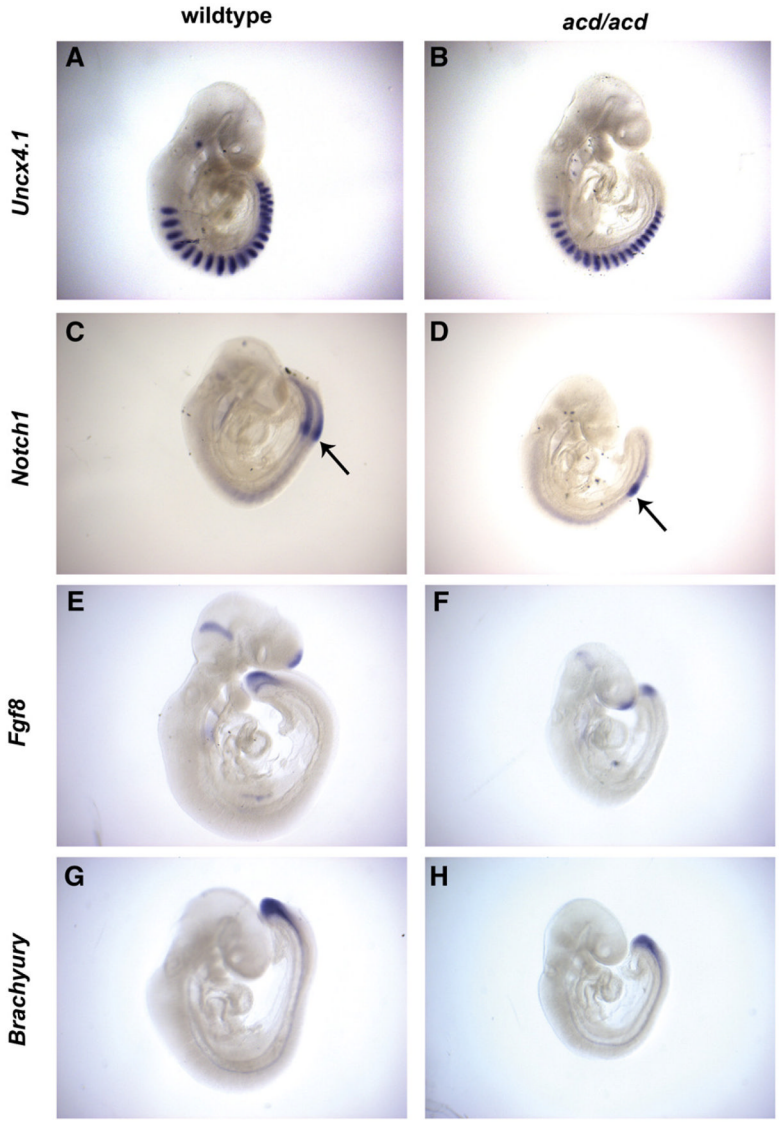


**Fig. 4.**

Somitogenesis and tail bud markers show normal expression patterning in *acd* mutant embryos. RNA *in situ* hybridization of wildtype and *acd* mutant littermate embryos at E9.5 using the somite marker *Uncx4.1* (A, B), the presomitic mesoderm marker *Notch1* (C, D), the tailbud marker *Fgf8* (E, F), and the T-box gene *brachyury* (G, H). Somite boundary is denoted by arrow in (C) and (D). In general, the expression patterns are normal in *acd* mutant embryos.

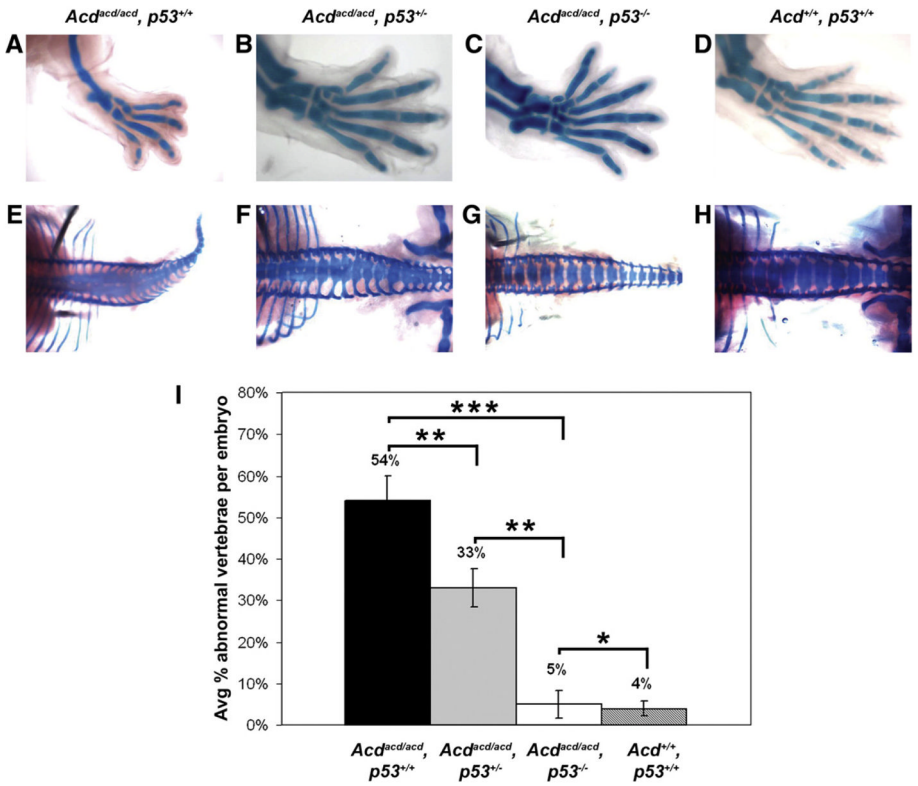


**Fig. 5.**

p53 deficiency rescues skeletal phenotype of *acd* mutant embryos. Skeletal staining of hindlimbs from *acd*×*p53* intercross embryos at E16.5 shows the absence of medial digit and tibia in *acd/acd*, $p53^{+/+}$ limb (A). Normal number of digits in *acd/acd*, $p53^{+/-}$ limb (B). Preaxial polydactyly is noted in *acd/acd*, $p53^{-/-}$ limb (C). Wildtype embryo limb pictured in panel (D). Skeletal staining of vertebral columns from *acd*×*p53* intercross embryos at E16.5 shows multiple vertebral fusions throughout the length of the spinal column in *acd/acd*, $p53^{+/+}$ embryo (E). Multiple vertebral fusions are also noted in *acd/acd*, $p53^{+/-}$ embryo (F), but fewer than *acd/acd*, $p53^{+/+}$ embryo. Complete lack of vertebral fusions in *acd/acd*, $p53^{-/-}$ embryo (G). Vertebral column of wildtype embryo shown in panel (H). Limbs were removed from embryos in (E) and (G) for photography. All photographs were taken at the same magnification. (I) Quantification of percent abnormal vertebrae in each embryo reveals dose-dependent reduction of abnormal vertebrae with increasing p53 deficiency. *Denotes lack of statistical significance ($p$=0.66), **denotes $p$<0.05, ***denotes $p$<0.0001.

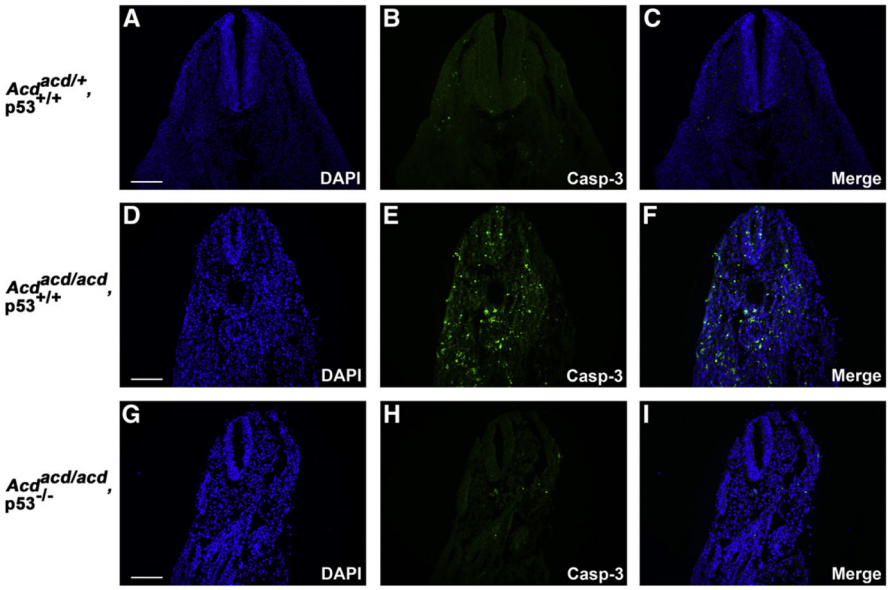


**Fig. 6.**

p53 deficiency rescues cellular apoptosis in *acd* mutant embryos. Immunofluorescence for cleaved caspase-3 (Casp-3) shows rare apoptotic cells in E10.5 wildtype (*acd*/+, $p53^{+/+}$ embryo tissue sections (A–C). A significant increase in Casp-3 staining is observed in *acd/acd*, $p53^{+/+}$ embryos (D–F). Only occasional Casp-3 positive cells are observed in *acd/acd*, $p53^{-/-}$ embryos (G–I), demonstrating rescue of apoptosis by p53 deficiency. Scale bars represent 100 μm.

**Table 1**

Genotypes reveal viability of *acd* mutant embryos on DW/J and C57BL/6 strains at E9.5 to E 11.5.

| Embryonic time point | Total number of embryos | +/+ | *acd*/+ | *acd/acd* | *p* value[a] |
|---|---|---|---|---|---|
| E9.5 | 59 | 11 | 30 | 18 | 0.5>*p*>0.3 |
| E10.5 | 61 | 11 | 35 | 15 | 0.5>*p*>0.3 |
| E11.5 | 65 | 15 | 36 | 14 | 0.8>*p*>0.7 |
| Total | 185 | 37 | 101 | 47 | 0.3>*p*>0.2 |
| Strain | | | | | |
| DW/J | 102 | 20 | 60 | 22 | 0.2>*p*>0.1 |
| B6 | 83 | 17 | 41 | 25 | 0.5>*p*>0.3 |
| Total | 185 | 37 | 101 | 47 | 0.3>*p*>0.2 |

[a] For predicted Mendelian ratios, df=2.

## Table 2

Genotypes of ($Acd^{acd/+} \times p53^{+/-}$) $F_2$ progeny at weaning.

| ***Acd* genotype**[a] | ***p53* genotype**[b] | | |
|---|---|---|---|
| | +/+ | +/− | −/− |
| +/+ | 10 | 23 | 4 |
| *acd*/+ | 26 | 44 | 15 |
| *acd/acd* | 0 | 0 | 0 |

$\chi^2$ 50.5, df=8, $p<0.0001$ for predicted Mendelian ratios.

[a] *acd* denotes mutant allele.

[b] – denotes *p53*-null allele.

## Table 3

Genotypes of ($Acd^{acd/+} \times p53^{+/-}$) $F_2$ progeny at E15.5–E16.5.

| ***Acd* genotype**[a] | ***P53* genotype**[b] | | |
|---|---|---|---|
| | **+/+** | **+/−** | **−/−** |
| +/+ | 8 | 30 | 6 |
| *acd*/+ | 16 | 51 | 21 |
| *acd/acd* | 7 | 23 | 9 |

$\chi^2$ 11.8, df=8, 0.05<*p*<0.2 for predicted Mendelian ratios.

[a] *acd* denotes mutant allele.

[b] – denotes *p53*-null allele.

**Table 4**

($Acd^{acd/+} \times p53^{+/-}$) intercross embryo hindlimb phenotypes.

| Genotypes (*Acd, p53*) | No. of embryos | No. of hindlimbs | Bifid digit | Polydactyly | Normal | Hypoplastic digits | Absent digits | Absent tibia[a] |
|---|---|---|---|---|---|---|---|---|
| +/+, +/+ | 8 | 16 | – | – | 16 (100%) | – | – | – |
| +/+, +/− | 30 | 60 | – | – | 60 (100%) | – | – | – |
| +/+, −/− | 6 | 12 | – | – | 12 (100%) | – | – | – |
| *acd*/+, +/+ | 16 | 32 | – | – | 32 (100%) | – | – | – |
| *acd*/+, +/− | 51 | 102 | – | – | 102 (100%) | – | – | – |
| *acd*/+, −/− | 21 | 42 | – | – | 42 (100%) | – | – | – |
| *acd*/acd, +/+ | 7 | 14 | – | – | 7 (50%) | 5 (35.7%) | 2 (14.3%) | 2 (14.3%) |
| *acd*/acd, +/− | 23 | 46 | 3 (6.5%) | – | 37 (80.4%) | 4 (8.7%) | 2 (4.4%) | 3 (6.5%) |
| *acd*/acd, −/− | 9 | 18 | 4 (22.2%) | 11 (61.1%) | 3 (16.7%) | – | – | – |
| Total | 171 | 342 | | | | | | |

Numerical values represent number and (percentage) of hindlimbs with each phenotype, – indicates 0 embryos with phenotype.

[a]Only found in the presence of hypoplasia or absent digit.